https://doi.org/10.1016/j.jpowsour.2020.229192

Unravel the influences of Ni substitution on Co-based electrodes for rechargeable alkaline Zn-Co batteries

Wenxu Shang[a], Wentao Yu[a], Xu Xiao[a], Yanyi Ma[a], Peng Tan[a*], Meng Ni[b*]

[a.] Department of Thermal Science and Energy Engineering, University of Science and Technology of China (USTC), Hefei 230026, Anhui, China.

[b.] Department of Building and Real Estate, Research Institute for Sustainable Urban Development (RISUD), Research Institute for Smart Energy (RISE), The Hong Kong Polytechnic University, Hung Hom, Kowloon, Hong Kong, China.

* Corresponding authors:
Email: pengtan@ustc.edu.cn (Peng Tan)
Email: meng.ni@polyu.edu.hk (Meng Ni)

Abstract: The performance of Zn-Co batteries is hindered by some critical issues, such as the low electric conductivity and poor valence-change ability, restricting the utilization of the active material. This study aims at improving the electrochemical performance of the battery via substituting Ni on the Co_3O_4 electrode. A novel multiple self-assembled nanowire-nanosheet structure is constructed with the substitution of 10% Ni, and the high electric conductivity and decent valence change-ability push the electrode to the top-tier among reported Zn-Co batteries, including the high capacity of 272 mAh g^{-1}, high energy density of 448 Wh kg^{-1}, and excellent rate performance with a capacity retention ratio of 72.5% after even 40-fold increase of the current density. In terms of the cycle stability, it can operate well with a capacity retention ratio of 85.3% before the 1000^{th} cycle, while dramatically decay in the subsequent cycles. More importantly, to illuminate the role of Ni substitution on the capacity decay, a systematic investigation on the Ni substituted Co_3O_4 electrode is conducted for the first time. The capacity decay mechanism is proposed as the decreased low valence species, microstructure collapse, and irreversible phase

transition with an increase of the Ni substitution ratio. This work offers insights to develop high-performance and durable electrodes for Zn-Co batteries.

Keywords: Zn-Co battery, Cobalt oxide, Ni substitution, electrochemical performance, decay mechanism

1. Introduction

Fast energy consumption requires new energy storage systems. Battery, as one kind of promising candidates, is getting increasing attention in recent years. Representatively, Li-ion batteries have already been commercialized successfully due to the decent energy density, long cycle time, and high operation voltage [1–3]. Unfortunately, owing to the use of organic solvents and lithium-based active materials, safety issues are challenging for further development [4,5]. Recently, the research on Zn-based batteries has bloomed for the following reasons [6–11]. Firstly, stable zinc metal and aqueous electrolytes ensure intrinsic safety. Secondly, the earth-abundant zinc metal and cheap electrolyte guarantee a reasonable cost. Thirdly, the Zn electrode owes a high theoretical capacity of 820 mAh g^{-1}, enabling the potential of a Zn-based battery to achieve remarkable practical capacity.

One of the huge families of Zn-based batteries, the Zn-Co battery has gained the emerging interest [12–15]. In the form of transition metal oxidation, Co_3O_4 can exhibit a high theoretical capacity (446 mAh g^{-1}). When paired with a Zn electrode, the battery can operate at a high voltage of 1.8 V. The first Zn-Co battery is reported by Wang et al. [15] using the ultrathin porous Co_3O_4 nanosheet, and the capacity can reach 160 mAh g^{-1} with an energy density of 241 W h g^{-1}. In terms of cycling stability,

the battery can operate 2000 cycles with a capacity decay ratio of 20%. Subsequently, Tan et al constructed a Zn-Co battery with Co_3O_4 nanowire, which delivers a higher capacity of 173.6 mAh g^{-1} with a capacity decay ratio of 15.9% after 1000 cycles [16]. Considering the difference between the reported capacities and the theoretical capacity of 446 mAh g^{-1}, the utilization ratio of the active material is relatively low, which may be triggered by the poor electric conductivity and unsatisfactory electrochemical reaction surface. To this end, Shang et al. tuned the microstructure of Co_3O_4 to obtain a heterogeneous porous nanowire, and the battery can exhibit a decent capacity of 230 mAh g^{-1}, a good rate performance with the capacity retention ratio of 62.6% after the 20-fold increase of the current density [17]. Further, through introducing oxygen defects into Co_3O_4 nanosheet, Lu et al. fabricated a battery with a capacity of 240.8 mAg h^{-1} and an energy density of 295.5 Wh kg^{-1} [14]. However, the capacity value (240.8 mAh g^{-1}) is also only half of the theoretical value. Hence, limited by the intrinsic low conductivity and spinel structure, a further increase in the capacity is difficult by simply modifying the microstructure only.

The partial substitution of Co by the other transition metallic cation (e.g., Cu^{2+}, Ni^{2+}, Mn^{2+}, and Fe^{2+}) is a valid strategy to improve the electrochemical performance through enhancing electronic conductivity and tuning the spinel structure [18–22]. Especially, Ni substitution is an effective strategy applied in various fields. For example, when substituting the Co^{2+} by Ni^{2+}, Li et al. obtained a supercapacitor with a specific capacity of 1828 F g^{-1}, substantially higher than the pristine value (948 F g^{-1}) [23]. Tan et al. reported that the Ni substitution in MCo_2O_4 (M=Co, Ni, and Fe)

delivers the best activity for both oxygen reduction reaction (ORR) and oxygen evolution reaction (OER) [24]. Bothra et al. proved that the catalytic activity of the oxygen reduction is related to the Ni substitution ratio in $Ni_xCo_{3-x}O_4$, in which the sample with x=0.25 exhibited the lowest overpotential (0.53 V) compared to the one with x=0.5 (0.61 V) and the pristine Co_3O_4 (0.76 V) [25]. Further, Lu et al. investigated the influence of the different atomic ratios of Ni to Co on the oxygen evolution, and they indicated that the morphology can be tuned from nanowire to nanoplate when the atomic ratio increases from 1:1 to 4:1, and the one with the ratio of 1:1 exhibits the best catalytic activity [26]. Our previous work also indicated that $NiCo_2O_4$ can exhibit the excellent electrochemical performance of a high capacity of 230.1 mAh g^{-1} and an energy density of 301.3 Wh kg^{-1} [27]. However, the microstructure of Co_3O_4 changed after the Ni substitution, and the theoretical capacity also decreases from 446 to 335 mAh g^{-1} due to the only one electron transfer ability of Ni. Besides, $NiCo_2O_4$ shows poor cycle stability with a capacity retention ratio of 63.23% after only 1000 cycles when compared to the Co_3O_4 electrode. Generally, the decay of a Zn battery is often attributed to the Zn electrode in most works with a simple assumption that the positive electrode is stable, while the change in the positive electrode, especially with other metal substitution during cycling, has never been reported. Hence, a systematic study is in great demand to unveil the underlying mechanism.

Herein, to systematically investigate the influences of the Ni substitution on the electrochemical behaviors of Co_3O_4 in Zn-Co batteries, different Ni substitution ratios

(0%, 5%, 10%, and 15%) were applied to prepare the samples. First, the morphology, element composition, and surface state were characterized. Then, the electrochemical performance was carefully measured in a battery system, including the redox reaction activity, discharge-charge capacity, and rate performance. Among them, the best sample was selected for further evaluation. Moreover, the cycle stability of these samples was tested, and the electrodes after cycle were characterized. For the first time, the decay of the Co_3O_4 electrode with Ni substitution during the long-term cycles was studied, and the underlying mechanism was proposed.

2. Experimental

2.1 Fabrication of Ni-substituted samples

The Co_3O_4 samples with different Ni substitution ratios were synthesized by hydrothermal reactions as previously reported [27]. Firstly, the Ni foam (3 cm × 5 cm) was cleaned thoroughly by acetone solution, 1 M HCl solution, and deionized water in sequent, and dried 2 h in a vacuum chamber to avoid oxidation. To fabricate the samples with different Ni substitution ratios (0%, 5%, 10%, and 15%), 1, 0.95, 0.9, and 0.85 mmol of $Co(NO_3)_2 \cdot 6H_2O$ paired with 0, 0.05, 0.1, and 0.15 mmol of $Ni(NO_3)_2 \cdot 6H_2O$, respectively, 4.5 mmol of NH_4F, and 8 mmol of $CO(NH_2)_2$ were dissolved into 40 mL of water. Then, the solution was poured into an autoclave of 50 mL, and the prepared Ni foam was fully immersed in it. After maintained under 120 ^oC for 9 h and returned to ambient temperature, the precursor was washed, dried. Finally, it was calcined in the air under 350 ^oC for 3 h with a heating rate of 1 ^oC min^{-1}. All samples have a mass loading of ~2.2 mg cm^{-2}. For the sake of convenience,

the obtained samples with different Ni substitution ratios (0%, 5%, 10%, and 15%) in the following parts were named as Co_3O_4, 5%-Ni, 10%-Ni, and 15%-Ni, respectively.

2.2 Material characterization

The material characterization was carried out at the Experimental Center of Engineering and Material Sciences in USTC, including the X-ray powder diffraction (XRD, smartlab) with a Cu-Kα source operating at 45 keV, scanning electron microscopy (SEM, XL-30 ESEM) under an acceleration voltage of 3 kV, field emission transmission electron microscopy (TEM, JEM-2100F) with a LaB6 filament at 200 kV, high-resolution TEM (HRTEM) images, energy dispersive spectroscopy (EDS) mapping, X-ray photoelectron spectroscopy (XPS, ESCALASB 250 Xi, Thermo Scientific, USA) using Al monochromatic X-ray at a power of 150 W, and the specific surface areas and the corresponding pore volumes (Tristar II 3020M surface area and porosity analyzer).

2.3 Electrochemical measurements

To assemble the battery, the positive electrode was pouched from the as-treated sample with a diameter of 10 mm, the negative electrode was a Zn plate with a thickness of 0.5 mm, and the electrolyte was 6 M KOH with 0.2 M $Zn(Ac)_2$ solution. First, the cycle voltammetry (CV) was tested by an electrochemical workstation (Solartron EnergyLab) in the potential region from 1.20 to 1.95 V (vs. Zn) with the scan rates from 1 to 20 mV s^{-1}. Subsequently, the battery behaviors were tested at the current densities of 0.5, 1, and 2 A g^{-1} in the voltage range of 1.4 and 1.9 V. As for the full-cell behavior, the rate performance was measured at 0.25, 0.5, 1, 2, 4, 6, 8, and 10

A g^{-1}, and the cycle stability was conducted at 2 A g^{-1}.

3. Results and discussion

3.1 Characterization of Ni-substituted samples

Different substitution ratios of nickel (0%, 5%, 10%, and 15%) in Co_3O_4 were conducted, and the XRD patterns in Fig. 1 shows that all sample is Co_3O_4 (PDF #42-1467), suggesting that the spinal structure can be well retained after the Ni substitution. Using the same synthetic method, the morphology of the pristine Co_3O_4 was reported to be the nanowire [17]. For the sample with different Ni substitution ratios, the SEM and TEM images are illustrated in Fig. 2. Interestingly, a new microstructure is presented and changes dramatically with the ascending substitution ratio. At the substitution ratio of 5% (Figs. 2a and 2b), the sample presents a uniform self-assembled structure grown on Ni foam with the nanowires aggregated into nanosheet. At the ratio of 10% (Figs. 2d and 2e), the amount of nanowires decreases while the nanosheets become denser. When the ratio reaches 15% (Figs. 2g and 2h), the layered nanosheets almost take up and only some nanowires retain. The TEM images are consistent with this observation. When the ratio increases, the number of nanowires decreases, which are embedded into the nanosheet and almost disappear at 15% (Figs. 2c, 2f, and 2i). The high-resolution TEM images in Fig. S1 indicates the lattice spacings of 0.28, 0.47, and 0.2 nm, which are indexed to the (220), (311), and (400) planes of spinel Co_3O_4, respectively, consistent with the XRD results. Moreover, the EDS mapping images of 10%-Ni in Fig. S2 shows the element distribution of Co, Ni, and O in both nanowires and nanosheets, which can validate the success of Ni

substitution. Fig. 2j depicts the morphology variation from wire to sheet with increasing substitution ratio. It is speculated that after Ni substitution, the nanowires on the Ni foam integrate together into the nanosheet from the bottom. With the ascending of the substitution ratio, the fusion degree increases and the nanosheets grow denser, while the nanowires disappear gradually. When the Ni substitution ratio reaches a relatively high value (i.e., 15%), the nanowires almost merge together, presenting the morphology of the entire nanosheet. As shown in Fig. S3, the specific surface areas are calculated to be 9.81, 8.42, 8.2, and 7.67 $m^2 g^{-1}$, respectively, which decreases as the Ni substitution ratio increasing, consistent with the morphology variation.

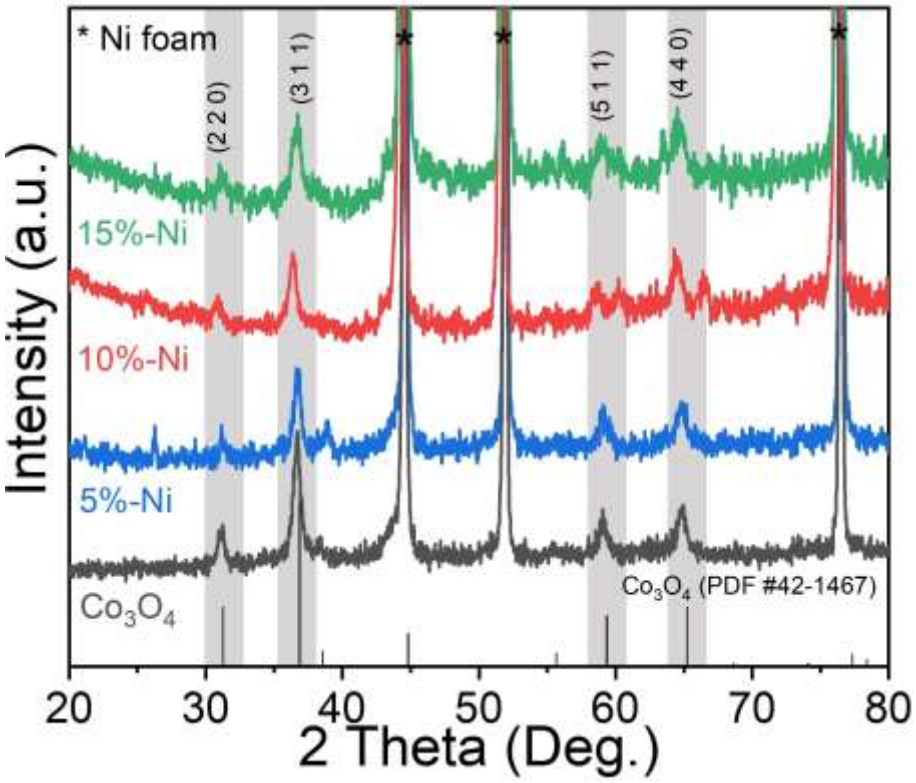

Fig. 1. XRD patterns of the samples with different Ni substitution ratios.

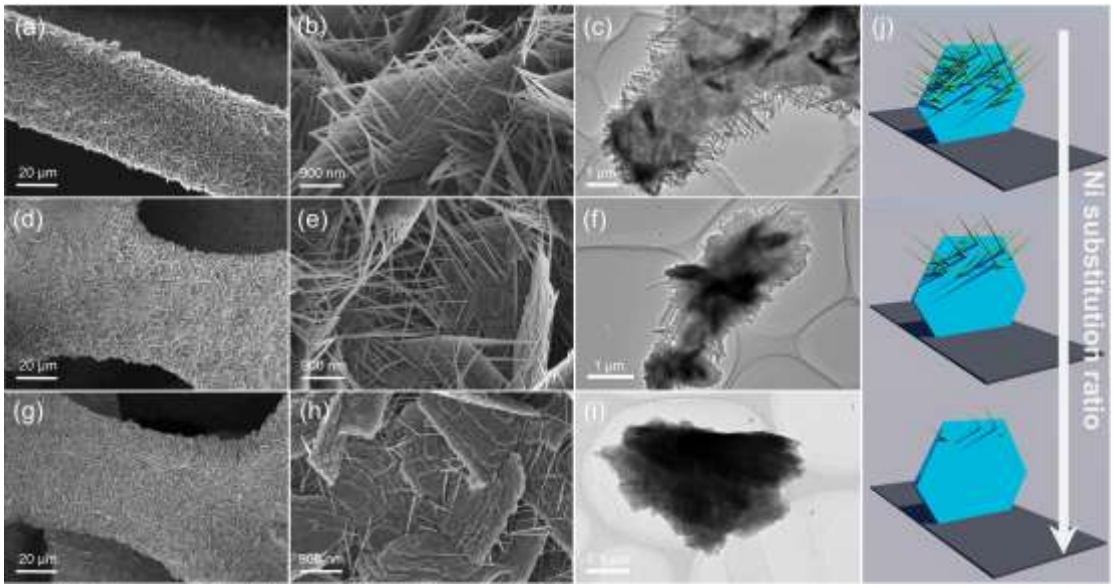

Fig. 2. Microstructure and morphology of the samples with different Ni substitution ratios. (a-c) 5%-Ni: (a, b) SEM images at different magnifications; (c) TEM image. (d-f) 10%-Ni: (d, e) SEM images at different magnifications; (f) TEM image. (g-i) 15%-Ni: (g, h) SEM images at different magnifications; (i) TEM image. (j) schematic illustration of the morphology variation.

The element composition and oxidation states of different samples under the discharged state were unveiled by XPS. As shown in Fig. 3a, the curve of the Co 2p spectra can be fitted into six peaks: the two peaks at 796.4 and 781.3 eV correspond to Co^{2+}, the two peaks at 794.9 and 779.7 eV correspond to Co^{3+}, while the other two at 805.2 and 788.52 eV correspond to the satellite peaks. For the Ni 2p spectra in Fig. 3b, similarly, the peaks at 871.8 and 853.2 eV correspond to Ni^{2+}, the peaks at 873.4 and 855.7 eV correspond to Ni^{3+}, and the other two at 879.1 and 861.4 eV correspond to the satellite peaks. Based on the fitting results, the ratio of Co^{2+}/Co^{3+} and Ni^{2+}/Ni^{3+} can be calculated as summarized in Table S1. In detail, for Co_3O_4, 5%-Ni, 10%-Ni, and 15%-Ni, the ratios of Co^{2+}/Co^{3+} are 1.205, 1.32, 1.441, and 1.344, respectively.

Hence, the ratio of Co^{2+} was lifted after Ni doping, especially at 10%, indicating its greater valance changeability. While the ratios of Ni^{2+}/Ni^{3+} are 0.191, 0.297, and 0.358 for the 5%-Ni, 10%-Ni, and 15%-Ni, respectively. Therefore, the ratio of Ni^{2+} can also raise ostensibly as an increase in the Ni substitution ratio.

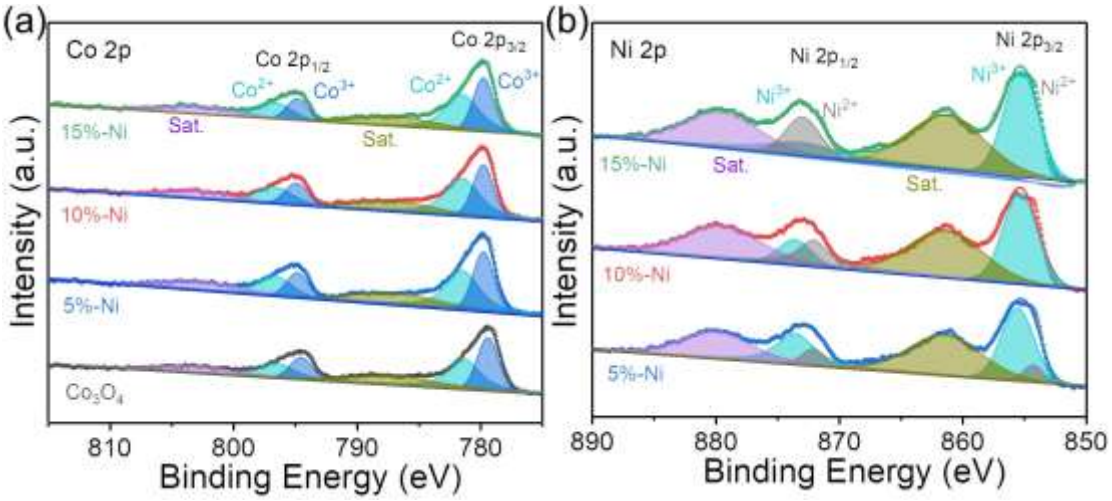

Fig. 3. XPS spectra of the samples with different Ni substitution ratios. (a) Co 2p and (b) Ni 2p.

3.2 Electrochemical performance of Ni-substituted samples

The electrochemical tests were applied for each sample in a two-electrode system. The CV curves at different scan rates from 1 to 20 mV s^{-1} were tested to examine the redox behaviors, as shown in Fig. S4. Fig. 4a compares their CV curves at 10 mV s^{-1}. It is worth noting that in an alkaline Zn-air battery, the oxygen equilibrium potential is 1.65 V (vs. Zn). When the charge voltage is higher than 1.65 V, the oxygen evolution reaction (OER) may occur and the gaseous oxygen bubbles may absorb on the surface of the electrode, decreasing the reaction surface area and leading to the loss of redox capacity. While in the present work, the OER is not apparent even the potential is higher than 1.95 V as shown from the CV curves,

indicating that the OER has limited effects on the redox capacity. For the oxygen reduction reaction (ORR), due to the lack of three-phase (i.e., solid, liquid, and gas) interfaces on the present electrode and the closed structure of the battery, the ORR can hardly occur and have almost no effects on the redox capacity. The peaks of the samples substituted by Ni are higher than the pristine one. In detail, the peak value of different samples can be ranked as: 10% > 15% > 5% > 0%. Moreover, their capacitance values are illustrated in Fig. 4b. At 1 mV s^{-1}, the values are 1989.2, 2697.3, 3346, and 3074.7 F g^{-1}, respectively. Especially, the 10%-Ni sample exhibits the highest value, which may be ascribed to its excellent valance changeability and good electric conductivity. To verify this result, the samples were tested in a battery system. Different from the reported Zn-ion batteries, the reaction process during charge/discharge does not involve the intercalation/extraction process of Zn ions [13]. Instead, it involves the redox reactions of the active material, which can be proposed as follows:

$$Co_3O_4 + OH^- + H_2O \underset{\text{Discharge}}{\overset{\text{Charge}}{\rightleftharpoons}} 3CoOOH + e^- \quad (1)$$

$$CoOOH + OH^- \underset{\text{Discharge}}{\overset{\text{Charge}}{\rightleftharpoons}} CoO_2 + H_2O + e^- \quad (2)$$

$$NiO + OH^- \underset{\text{Discharge}}{\overset{\text{Charge}}{\rightleftharpoons}} NiOOH + e^- \quad (3)$$

For the reaction process in the negative electrode, it is the zinc oxidation and the zincate reduction as follows:

$$Zn(OH)_4^{2-} + 2e^- \underset{\text{Discarge}}{\overset{\text{Charge}}{\rightleftharpoons}} Zn + 4OH^- \quad (4)$$

Hence, Zn ions do not transfer to the positive electrode. To further confirm this point, we measured the EDS results of the 10%-Ni sample under the discharged state,

as shown in Figs. S5 and S6, which proves that only Ni, Co, and O exist in the electrode. Fig. 4c displays the discharge-charge voltage curves at the current density of 0.5 A g^{-1}. For the samples with different Ni substitution ratios (0%, 5%, 10%, and 15%), the discharge capacities are 218.6, 229.4, 265.0, and 249.6 mAh g^{-1}, respectively, and the charge values are 230.8, 239.3, 280.1, and 258.6 mAh g^{-1}, respectively. The corresponding coulombic efficiency is 94.7%, 95.9%, 94.6%, and 96.5%, respectively, which are all close to 100%. To compare the rate performance of the samples, 1 and 2 A g^{-1} were also tested (Figs. 4d and 4e). With the current density increases, the discharge capacity decreases due to the polarization, while the shape of these charge/charge curves is similar to one another. Fig. 4f summarizes their discharge capacities at different current densities (0.5, 1, and 2 A g^{-1}). The corresponding capacity values have been marked in detail. Based on the results, the capacity retention ratios for these samples are 94.2%, 93.4%, 95.7%, and 93.2%, respectively, and the 10%-Ni sample achieves the best performance.

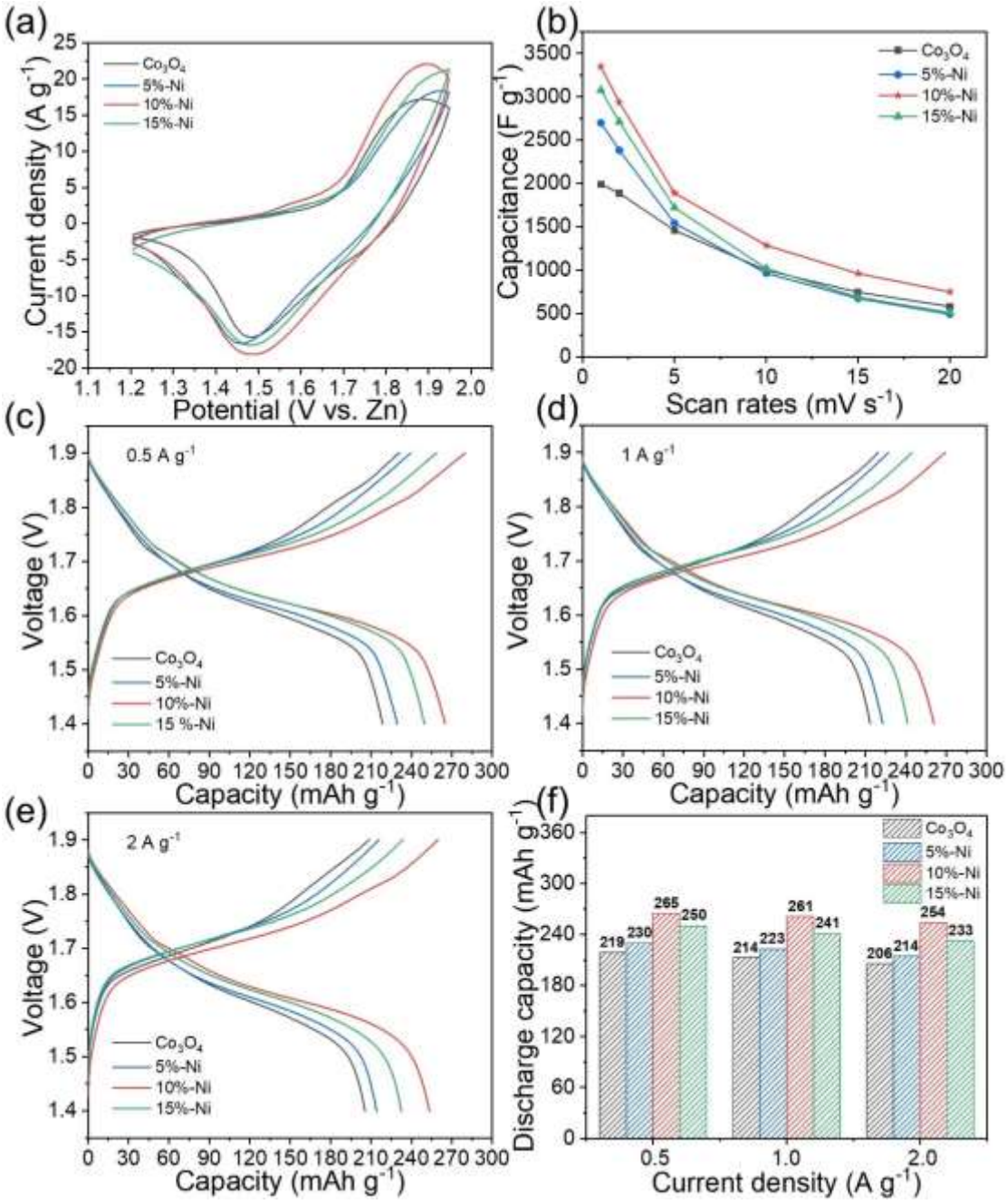

Fig. 4. Electrochemical performance of Zn-Co batteries with the samples of different Ni substitution ratios. (a) CV curves, (b) specific capacitance values at various scan rates, (c-e) galvanostatic charge-discharge voltage curves: (c) 0.5, (d) 1, and (e) 2 A g^{-1}, (f) comparison on the discharge capacity values.

Hence, the 10%-Ni sample was selected for further electrochemical evaluations. Figs. 5a and 5b illustrate its discharge-charge curves at various current densities. With

the current density increasing from 0.25 to 4 and even 10 A g^{-1}, the discharge capacity decreases from 272.0 to 238.7 and 197.1 mAh g^{-1}, with the capacity retention ratio of 72.5% even at the 40-fold current density. Besides, the energy density decreases from 448 to 313.4 Wh kg^{-1}, and the corresponding energy efficiency turns from 90.4% to 87.1%. In comparison, the capacity of the Ni-substitution Co_3O_4 (272.0 mAh g^{-1}) shines among the previously reported positive materials in alkaline Zn batteries [14–17,27–33] (Fig. 6a). Significantly, the rate performance is pretty better than other previously reported Co_3O_4-based material, such as the Co_3O_4 nanowires@Ni foam (34% from 1 to 7.5 A g^{-1}) [16], Co_3O_4 nanosheet@Ni foam (48% from 1 to 10 A g^{-1}) [15], heterogeneous porous nanowire Co_3O_4@Ni foam (62.6% from 0.5 to 10 A g^{-1}) [17], and ultrathin defect-rich Co_3O_4 nanosheet (40.8% from 4 to 40 mA cm^{-2}) [14]. The high capacity and comparable rate capability may be ascribed to the unique structure, surface state, and good electric conductivity. Firstly, the multiple self-assembled nanowire-nanosheet structure can exhibit a high surface area for reaction and porous structure for ion transport. Secondly, the high amount of Co^{2+} and Ni^{2+} increases the valence-change ability, promoting the utilization ratio of the active material. Thirdly, the partial substitution (e.g., 10%) instead of forming $NiCo_2O_4$ can maintain the electron transfer ability of cobalt, ensuring the high theoretical capacity [34]. Fourthly, the electric conductivity can be lifted after rational Ni substitution, accelerating the electron transfer [23,35,36].

To further evaluate the cycle stability, the battery was cycled at 2 A g^{-1}. Interestingly, the capacity retention can remain well before the 1000^{th} cycle, while

drops dramatically after that, and finally reaches 63.9% in the 2000th cycle (Fig. 5c). It is worth noting that this result is even inferior to that of the pristine Co_3O_4 (66.8% after 3000 cycles) [17]. To estimate the cycle performance detailedly, the capacity retention ratios at different cycle numbers (500th, 1000th, 1500th, and 2000th cycles) were listed to compare with other reported Zn batteries (Fig. 6b). The Ni-substitution Co_3O_4 shows the decent cycle performance (85.3% at the 1000th cycle) before the 1000th cycle, better than most previous electrode, such as NiO-CNTs (65% after 500 cycles) [28] and $NiCo_2O_4$ nanowire (63.23% after 1000 cycles) [27]. However, after the 1000th cycle, the capacity retention ratio is at a disadvantage, such as CC-CF@NiO (72.9% after 2400 cycles) [29] and heterogeneous Co_3O_4 nanowire (66.8% after 3000 cycles) [17].

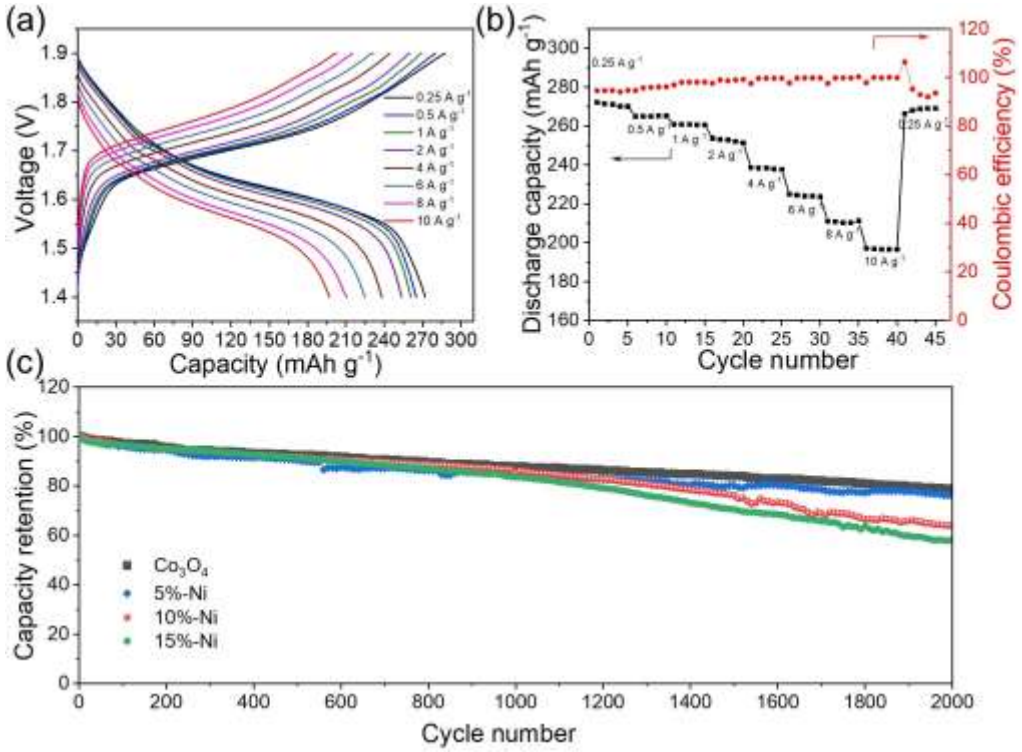

Fig. 5. Full-cell performance of the Zn-Co battery with the 10%-Ni sample. (a) the charge-discharge curves at the current density ranging from 0.25 to 10 A g^{-1}, (b)

capacity values and corresponding coulombic efficiency, (c) the capacity retention ratios and the corresponding coulombic efficiency with different Ni substitution ratios during 2000 cycles at 2 A g^{-1}.

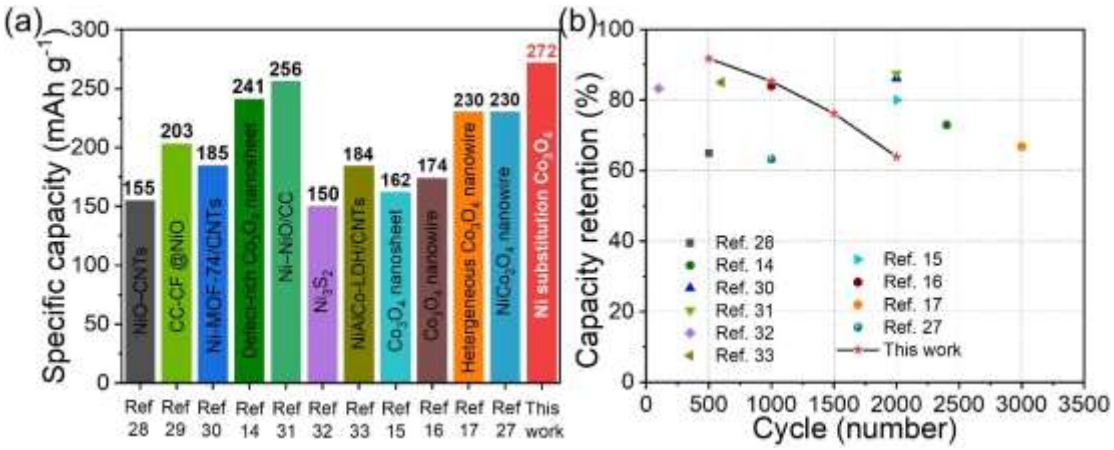

Fig. 6. Performance comparisons of Zn-Co batteries with different positive electrode materials. (a) discharge capacity values and (b) capacity retention ratios at different cycle numbers.

3.3 Effects of Ni substitution on cycling stability

In view of the unsatisfactory cycling stability compared to other electrodes, further investigation is conducted. Our previous work indicated that the pristine Co_3O_4 can deliver decent cycling stability (66.8% after even 3000th cycle) [17], while the $NiCo_2O_4$ electrode has poor stability (63.23% after 1000th cycle) [27]. Hence, it can preliminarily speculate that cycling stability is relevant to Ni substitution. To further validate our conjecture, the samples with different Ni substitution ratios (i.e., 0%, 5%, 10%, and 15%) were assembled into batteries and cycled in the same manner (i.e., 2 A g^{-1} and 2000 cycles), and the voltage curves are shown in Fig. S7. As illustrated in Fig. 5c, a clear difference in the cycle curves is presented. The capacity retention ratios remain well and the curves almost overlap before the 1000th cycle.

However, four curves start to change dramatically in the subsequent cycle: with the ascending of Ni substitution ratio, the cycle stability degrades visibly. In detail, the capacity retention ratio at the 2000^{th} cycle drops from 78.57% to 76.05%, 63.9%, and 58.23% as the Ni substitution ratio rises, consistent with our conjecture. Afterward, the electrodes after cycle were picked for in-depth characterization. The XRD in Fig. S8 indicates that the electrode is still Co_3O_4 while the peak is no longer clear, especially the ones with the Ni substitution ratios of 10% and 15%. Besides, the peak at 25.9^o indicates the appearance of NiOOH after cycle. Furthermore, the microstructure changes severely with the Ni substitution ratio rises (Fig. 7). As shown from the SEM images, the Co_3O_4 (Figs. 7a and 7b) and the 5%-Ni (Figs. 7c and 7d) samples after cycle display few changes, and the nanowires and nanosheets retain well. In comparison, the great change appears on the 10%-Ni (Figs. 7e and 7f) and 15%-Ni (Figs. 7g and 7h) samples, from which the nanosheets seem to break up and turn into nanowires, which leads to an unstable structure during operation. More importantly, the microstructure change has a great influence on the surface area and porous structure, affecting reaction interface and ion transport.

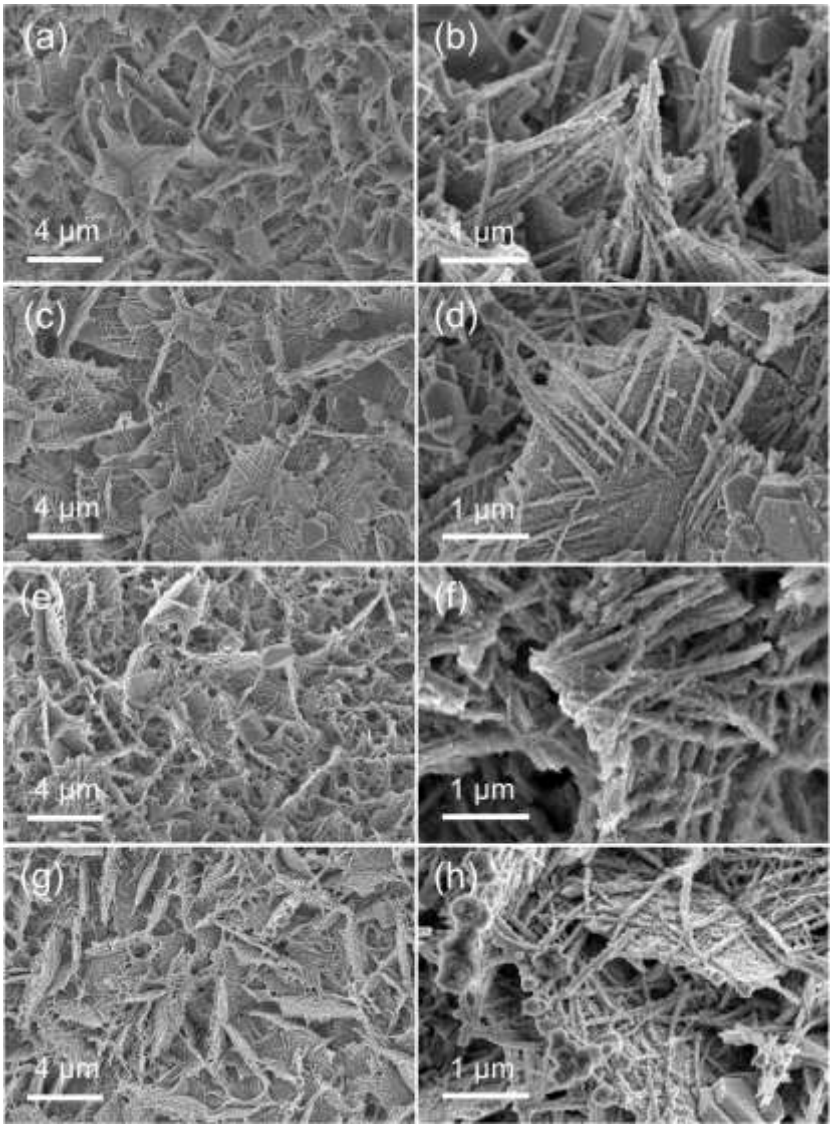

Fig. 7. SEM images at different magnifications of the samples with different Ni substitution ratios after 2000th cycle: (a, b) Co_3O_4, (c, d) 5%-Ni, (e, f) 10%-Ni, and (g, h) 15%-Ni.

Additionally, the variation in the surface states of the samples under the discharged state is reflected by the element composition. As the XPS spectra shown in Fig. 8, and the corresponding ratios are summarized in Table S2. After the cycle, the ratio of Co^{2+}/Co^{3+} turns to 0.945, 1.186, 1.208, and 0.803 for Co_3O_4, 5%-Ni, 10%-Ni, and 15%-Ni, respectively (Fig. 8a). Hence, the ratio of Co^{2+}/Co^{3+} decreases after a long cycle, especially for the 15%-Ni sample which changes from 1.344 to 0.803,

reducing the valence changeability of Co dramatically. As for the Ni 2p, the ratio of Ni^{2+}/Ni^{3+} also drops from 0.191 to 0.149, 0.297 to 0.0759, and 0.358 to 0.1176 for the 5%-Ni, 10%-Ni, and 15%-Ni, respectively (Fig. 8a). Thus, the value drops severer as the Ni substitution ratio increasing, so that the valence changeability of Ni also decreases dramatically, consistent with the XRD results.

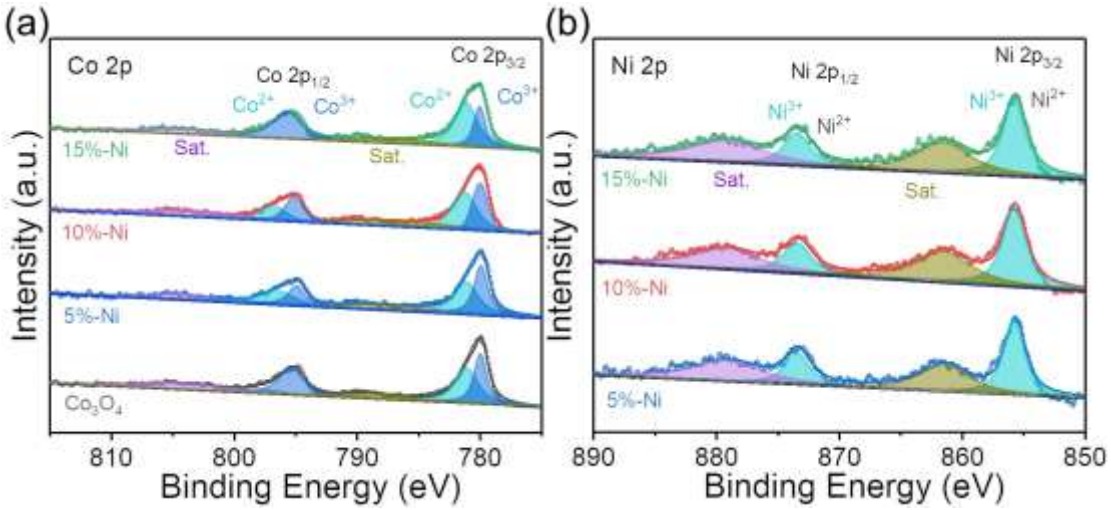

Fig. 8. XPS spectra of the samples with different Ni substitution ratios after the 2000th cycle. (a) Co 2p and (b) Ni 2p.

Based on the above results, we suspected that the decay of the electrode, especially at the high Ni substitution ratios, may be triggered by three aspects: I) the decline in the content of Co^{2+} and Ni^{2+} reduces the redox reaction ability, lowering the utilization ratio of the active material; II) the collapse of the microstructure ruins the pore structure, cause the particle aggregation, and decrease the electrochemical active surface area and impede the ion transport; III) the spinel structure of Co_3O_4 may be unstable with the increasing Ni content during the cycle, and some irreversible phase transition may also occur. To further investigate the transformation of the crystal structure, the O 1s XPS spectra of the samples before and after the 2000th cycle is

presented (Fig. S9). After the cycle, even the shape of the XPS curves change and the proportion of oxygen defects increases dramatically as the Ni substitution ratio increases, which verifies the transformation of the crystal structure. Since some works have reported the unstable phase transition from β-$Ni(OH)_2$ to β-NiOOH, the change on the spinel structure of the Co_3O_4 with Ni substitution after the cycle may also lead to the unstable phase transition due to the heterogeneous doping [37,38]. As for an idea to ameliorate the cycle stability, modifying the structure may be feasible, such as adding CNT, doping Al, or designing multilevel "core-shell" structure [33,38], which will be our future research topic.

4. Conclusions

In summary, the influences of different Ni substitution ratios (0%, 5%, 10%, and 15%) on the Co_3O_4 electrode in alkaline Zn-Co batteries have been investigated systematically. After Ni substitution, the morphology turned into a multiple self-assembled nanowire-nanosheet structure, and the nanosheet becomes denser as the ratio increases. The electrochemical test shows that the Ni substitution sample can deliver the high specific capacitance, especially the 10%-Ni sample exhibits a much higher value of 3346 F g^{-1} than the pristine one (1989.2 F g^{-1}). When served in a battery, the decent performance also makes the 10%-Ni sample top-tier among the previously reported Zn batteries, as reflected by an increase in the capacity of 272 mAh g^{-1} and an excellent rate capability with the capacity retention of 72.5% after even 40-fold increase of the current density. The great improvement relative to the pristine Co_3O_4 can be ascribed to the reasonable self-assembled structure, decent

valence-change ability, and optimal electric conductivity. As for the cycle stability, it can operate well with a capacity retention ratio of 85.3% before the 1000^{th} cycle, while dramatically decay in the subsequent cycles. To systematically investigate the influence of Ni substitution on the electrode decay, the cycle behaviors of the samples with different Ni ratios were also tested. With the increase of ratio from 0% to 5%, 10%, and 15%, the capacity retention decreases from 78.57% to 76.05%, 63.9%, and 58.23%, respectively. The characterization of the electrodes after cycle indicated that the decay may be triggered by the low valence species decrease, microstructure collapse, and the unstable crystal structure due to the irreversible phase transition. Hence, this work designs a promising positive electrode for a high-performance Zn-Co battery in the capacity and rate capability. More importantly, the decay mechanism in the positive electrode is spotlighted for the first time, paving a new avenue for future innovation on the positive electrode development for long-cycle stable Zn-Co batteries.

CRediT authorship contribution statement

Wenxu Shang: Conceptualization, Investigation, Methodology, Writing - original draft. **Wentao Yu:** Investigation, Methodology. **Xu Xiao:** Investigation, Methodology. **Yanyi Ma:** Validation, Formal analysis. **Peng Tan:** Conceptualization, Formal analysis, Writing - review & editing, Supervision, Project administration, Funding acquisition. **Meng Ni:** Writing - review & editing, Supervision, Funding acquisition.

Acknowledgments

P. Tan thanks the funding support from Anhui Provincial Natural Science Foundation (2008085ME155), CAS Pioneer Hundred Talents Program (KJ2090130001), USTC Research Funds of the Double First-Class Initiative (YD2090002006), Joint Laboratory for USTC and Yanchang Petroleum (ES2090130110), and USTC Tang Scholar. M. Ni thanks the funding support (Project Number: PolyU 152214/17E and PolyU 152064/18E) from Research Grant Council, University Grants Committee, Hong Kong SAR.

References

[1] D. Ouyang, M. Chen, Q. Huang, J. Weng, Z. Wang, J. Wang, A Review on the thermal hazards of the lithium-ion battery and the corresponding countermeasures, Appl. Sci. 9 (2019) 2483.

[2] Q. Wang, L. Jiang, Y. Yu, J. Sun, Progress of enhancing the safety of lithium ion battery from the electrolyte aspect, Nano Energy. 55 (2019) 93–114.

[3] H. Yang, H. Zhou, Halogen conversion-intercalation chemistry promises high energy density Li-ion battery, Sci. Bull. 64 (2019) 1393–1395.

[4] X. Han, L. Lu, Y. Zheng, X. Feng, Z. Li, J. Li, M. Ouyang, A review on the key issues of the lithium ion battery degradation among the whole life cycle, ETransportation. 1 (2019) 100005.

[5] K. Xu, Nonaqueous liquid electrolytes for lithium-based rechargeable batteries, Chem. Rev. 104 (2004) 4303–4417.

[6] X. Li, Y. Tang, H. Lv, W. Wang, F. Mo, G. Liang, C. Zhi, H. Li, Recent

advances in flexible aqueous zinc-based rechargeable batteries, Nanoscale. 11 (2019) 17992–18008.

[7] H. Li, L. Ma, C. Han, Z. Wang, Z. Liu, Z. Tang, C. Zhi, Advanced rechargeable zinc-based batteries: Recent progress and future perspectives, Nano Energy. 62 (2019) 550–587.

[8] Y. Li, J. Fu, C. Zhong, T. Wu, Z. Chen, W. Hu, K. Amine, J. Lu, Recent Advances in Flexible Zinc-Based Rechargeable Batteries, Adv. Energy Mater. 9 (2019) 1802605.

[9] P. Tan, B. Chen, H. Xu, H. Zhang, W. Cai, M. Ni, M. Liu, Z. Shao, Flexible Zn- and Li-air batteries: Recent advances, challenges, and future perspectives, Energy Environ. Sci. 10 (2017) 2056–2080.

[10] W. Shang, W. Yu, P. Tan, B. Chen, Z. Wu, H. Xu, M. Ni, Achieving high energy density and efficiency through integration: Progress in hybrid zinc batteries, J. Mater. Chem. A. 7 (2019) 15564–15574.

[11] Z. Chen, Q. Wang, X. Zhang, Y. Lei, W. Hu, Y. Luo, Y. Wang, N-doped defective carbon with trace Co for efficient rechargeable liquid electrolyte-/all-solid-state Zn-air batteries, Sci. Bull. 63 (2018) 548–555.

[12] L. Ma, S. Chen, H. Li, Z. Ruan, Z. Tang, Z. Liu, Z. Wang, Y. Huang, Z. Pei, J.A. Zapien, C. Zhi, Initiating a mild aqueous electrolyte Co_3O_4/Zn battery with 2.2 V-high voltage and 5000-cycle lifespan by a Co(iii) rich-electrode, Energy Environ. Sci. 11 (2018) 2521–2530.

[13] W. Shang, W. Yu, Y. Liu, R. Li, Y. Dai, C. Cheng, P. Tan, M. Ni,

Rechargeable alkaline zinc batteries: Progress and challenges, Energy Storage Mater. 31 (2020) 44–57.

[14] Y. Lu, J. Wang, S. Zeng, L. Zhou, W. Xu, D. Zheng, J. Liu, Y. Zeng, X. Lu, An ultrathin defect-rich Co_3O_4 nanosheet cathode for high-energy and durable aqueous zinc ion batteries, J. Mater. Chem. A. 7 (2019) 21678.

[15] X. Wang, F. Wang, L. Wang, M. Li, Y. Wang, B. Chen, Y. Zhu, L. Fu, L. Zha, L. Zhang, Y. Wu, W. Huang, An Aqueous Rechargeable Zn//Co_3O_4 Battery with High Energy Density and Good Cycling Behavior, Adv. Mater. 28 (2016) 4904–4911.

[16] P. Tan, B. Chen, H. Xu, W. Cai, W. He, M. Ni, In-situ growth of Co_3O_4 nanowire-assembled clusters on nickel foam for aqueous rechargeable Zn-Co3O4 and Zn-air batteries, Appl. Catal. B Environ. 241 (2019) 104–112.

[17] W. Shang, W. Yu, X. Xiao, Y. Ma, C. Cheng, Y. Dai, Microstructure-tuned cobalt oxide electrodes for high-performance Zn-Co batteries, Electrochim. Acta. 353 (2020) 136535.

[18] S. Ye, Y. Zhang, W. Xiong, T. Xu, P. Liao, P. Zhang, X. Ren, C. He, L. Zheng, X. Ouyang, Q. Zhang, J. Liu, Constructing tetrahedral CoO_4 vacancies for activating the high oxygen evolution activity of $Co_{3-x}O_{4-\delta}$ porous nanosheet arrays, Nanoscale. 12 (2020) 11079–11087.

[19] S. Liu, K.S. Hui, K.N. Hui, J.M. Yun, K.H. Kim, Vertically stacked bilayer $CuCo_2O_4$/$MnCo_2O_4$ heterostructures on functionalized graphite paper for high-performance electrochemical capacitors, J. Mater. Chem. A. 4 (2016)

8061–8071.

[20] H. Li, A. Vojvodic, J. He, X. Zheng, M. Zhou, M. García-Melchor, W. Wu, L. Cai, M. Bajdich, J. Wilcox, Enhancing Catalytic CO Oxidation over Co_3O_4 Nanowires by Substituting Co^{2+} with Cu^{2+}, ACS Catal. 5 (2015) 4485–4491.

[21] B. Chi, H. Lin, J. Li, Cations distribution of $Cu_xCo_{3-x}O_4$ and its electrocatalytic activities for oxygen evolution reaction, Int. J. Hydrogen Energy. 33 (2008) 4763–4768.

[22] Z. Yu, L. Chen, S. Yu, Growth of $NiFe_2O_4$ nanoparticles on carbon cloth for high performance flexible supercapacitors, J. Mater. Chem. A. 2 (2014) 10889–10894.

[23] S. Liu, D. Ni, H.F. Li, K.N. Hui, C.Y. Ouyang, S.C. Jun, Effect of cation substitution on the pseudocapacitive performance of spinel cobaltite MCo_2O_4 (M = Mn, Ni, Cu, and Co), J. Mater. Chem. A. 6 (2018) 10674–10685.

[24] P. Tan, Z. Wu, B. Chen, H. Xu, W. Cai, S. Jin, Z. Shao, M. Ni, Cation-substitution-tuned oxygen electrocatalyst of spinel cobaltite MCo_2O_4 (M = Fe, Co, and Ni) hexagonal nanoplates for rechargeable Zn-air batteries, J. Electrochem. Soc. 166 (2019) A3448–A3455.

[25] P. Bothra, S.K. Pati, Activity of Water Oxidation on Pure and (Fe, Ni, and Cu)-Substituted Co_3O_4, ACS Energy Lett. 1 (2016) 858–862.

[26] B. Lu, D. Cao, P. Wang, G. Wang, Y. Gao, Oxygen evolution reaction on Ni-substituted Co_3O_4 nanowire array electrodes, Int. J. Hydrogen Energy. 36 (2011) 72–78.

[27] W. Shang, W. Yu, P. Tan, B. Chen, H. Xu, M. Ni, A high-performance Zn battery based on self-assembled nanostructured $NiCo_2O_4$ electrode, J. Power Sources. 421 (2019) 6–13.

[28] X. Wang, M. Li, Y. Wang, B. Chen, Y. Zhu, Y. Wu, A Zn-NiO rechargeable battery with long lifespan and high energy density, J. Mater. Chem. A. 3 (2015) 8280–8283.

[29] J. Liu, C. Guan, C. Zhou, Z. Fan, Q. Ke, G. Zhang, C. Liu, J. Wang, A Flexible Quasi-Solid-State Nickel–Zinc Battery with High Energy and Power Densities Based on 3D Electrode Design, Adv. Mater. 28 (2016) 8732–8739.

[30] P. Man, B. He, Q. Zhang, Z. Zhou, C. Li, Q. Li, L. Wei, Y. Yao, A one-dimensional channel self-standing MOF cathode for ultrahigh-energy-density flexible Ni– Zn batteries, J. Mater. Chem. A. 7 (2019) 27217–27224.

[31] L. Li, L. Jiang, Y. Qing, Y. Zeng, Z. Zhang, L. Xiao, X. Lu, Y. Wu, Manipulating nickel oxides in naturally-derived cellulose nanofiber networks as robust cathodes for high-performance Ni–Zn batteries, J. Mater. Chem. A. 8 (2020) 565.

[32] P. Hu, T. Wang, J. Zhao, C. Zhang, J. Ma, H. Du, X. Wang, G. Cui, Ultrafast Alkaline Ni/Zn Battery Based on Ni-Foam-Supported Ni_3S_2 Nanosheets, ACS Appl. Mater. Interfaces. 7 (2015) 26396–26399.

[33] M. Gong, Y. Li, H. Zhang, B. Zhang, W. Zhou, J. Feng, H. Wang, Y. Liang, Z. Fan, J. Liu, H. Dai, Ultrafast high-capacity NiZn battery with NiAlCo-layered

double hydroxide, Energy Environ. Sci. 7 (2014) 2025–2032.

[34] H. Zhang, X. Zhang, H. Li, Y. Zhang, Y. Zeng, Y. Tong, P. Zhang, X. Lu, Flexible rechargeable Ni//Zn battery based on self-supported $NiCo_2O_4$ nanosheets with high power density and good cycling stability, Green Energy Environ. 3 (2017) 56–62.

[35] B. Jos´e, L. ´Alvarez-Contreras, L.-G. Janet, A. No´e, L.G. Arriaga, An advanced three-dimensionally ordered macroporous $NiCo_2O_4$ spinel as a bifunctional electrocatalyst for rechargeable Zn–air batteries, J. Mater. Chem. A. 478 (2020) 453007.

[36] Y. Li, Z. Zhou, G. Cheng, S. Han, J. Zhou, J. Yuan, M. Sun, L. Yu, Flower-like $NiCo_2O_4$–CN as efficient bifunctional electrocatalyst for Zn-Air battery, Electrochim. Acta. (2020) 135997.

[37] A. Van Der Ven, D. Morgan, Y.S. Meng, G. Ceder, Phase stability of nickel hydroxides and oxyhydroxides, J. Electrochem. Soc. 153 (2006) A210–A215.

[38] H. Zhang, R. Wang, D. Lin, Y. Zeng, X. Lu, Ni-based Nanostructures as High-performance Cathodes for Rechargeable Ni−Zn Battery, ChemNanoMat. 4 (2018) 525–536.